Journal of Fluorine Chemistry 178 (2015) 86–92

Contents lists available at ScienceDirect

Journal of Fluorine Chemistry

journal homepage: www.elsevier.com/locate/fluor

Structural transformation between two cubic phases of $(NH_4)_3SnF_7$

I.N. Flerov [a,b], M.S. Molokeev [a,c,*], N.M. Laptash [d], A.A. Udovenko [d], E.I. Pogoreltsev [a,b], S.V. Mel'nikova [a], S.V. Misyul [b]

[a] L.V. Kirensky Institute of Physics, Siberian Branch of RAS, 660036 Krasnoyarsk, Russia
[b] Siberian Federal University, 660074 Krasnoyarsk, Russia
[c] Far Eastern State Transport University, 680021 Khabarovsk, Russia
[d] Institute of Chemistry, Far Eastern Branch of RAS, 690022 Vladivostok, Russia

ARTICLE INFO

Article history:
Received 27 May 2015
Received in revised form 26 June 2015
Accepted 27 June 2015
Available online 30 June 2015

Keywords:
Cubic fluorides
Phase transitions
X-ray
Calorimetry
Crystal optics

ABSTRACT

Reinvestigations of the room temperature structure of ammonium heptafluorostannate $(NH_4)_3SnF_7 = (NH_4)_2SnF_6{\cdot}NH_4F = (NH_4)_3[SnF_6]F$ by both powder and single crystal X-ray diffractions have revealed that its real symmetry is $Pa{-}3$ ($Z = 8$) instead of $Pm{-}3m$ ($Z = 1$) suggested earlier. Polarizing optical observations, heat capacity, X-ray powder, and single crystal measurements were performed in a wide temperature range (100–420 K). A reversible structural phase transition of the first order between two cubic modifications $Pa{-}3 \leftrightarrow Pm{-}3m$ was found at about $T_0 = 360$ K. The structural models associated with partially disordered and totally ordered high and low temperature phases, respectively, comply with a large value of phase transition entropy.

© 2015 Elsevier B.V. All rights reserved.

1. Introduction

Ammonium heptafluorostannate(IV) $(NH_4)_3SnF_7$ belongs to a series of complex fluorides with a general chemical formula of $A_3F[MF_6]$, where A = NH_4, K, Rb, Cs; M = Si, Ge, Ti, Sn, Pb, Cr, Mn, Ni [1–7], containing "single" [8] or "free" or "independent" [9] fluoride ions along with complex octahedral $[MF_6]^{2-}$ anions. In this case, the compounds can be characterized as double salts as was initially considered for $(NH_4)_2SiF_6{\cdot}NH_4F$ [5]. Such compounds are thermodynamically stable but the energetic reasons for their formation are still unclear [8]. Recently, our pioneer complex study of physical properties of $(NH_4)_3TiF_7$ revealed a possibility to affect its crystal lattice stability by temperature and pressure variation [10–12]. It was shown that $(NH_4)_3TiF_7$ underwent the succession of two phase transitions (PT) $Pa{-}3$ (290 K) $\leftrightarrow$ $P4/mnc$ (358 K) $\leftrightarrow$ (unsolved tetragonal phase with the other 4/m point group symmetry), and the emergence of $(NH_4)_2TiF_6$ hexagonal phase due to partial thermal decomposition of $(NH_4)_3TiF_7$ was detected at its final heating. The $(Pa{-}3) \leftrightarrow (P4/mnc)$ PT was found to be reconstructive and rather unusual because the cubic phase of $(NH_4)_3TiF_7$ transformed into the tetragonal one upon heating.

The experimental study of $(NH_4)_3TiF_7$ as well as different room temperature symmetries of A_3MF_7 compounds [1–7,10–12] depending on the size of a central atom indicate to the significance of further investigations of this series of crystals. On the one hand, it is hoped to find other interesting successions of the symmetry change in such double fluorides. On the other hand, it is not improbable that such compounds can exhibit significant barocaloric effects due to large values of the entropy change at structural transformations as well as the shift of PT temperature under pressure as was observed for $(NH_4)_3TiF_7$ [12].

Analysis of the temperature–pressure phase diagram [12] showed that $(NH_4)_3TiF_7$ could undergo the direct $Pa{-}3 \leftrightarrow Pm{-}3m$ PT because two intermediate tetragonal phases disappeared under pressure. Since Sn and Pb ions have bigger ion radii than Ti ion, it can be assumed that the structures of $(NH_4)_3SnF_7$ and $(NH_4)_3PbF_7$ are affected by internal pressure and, thus, there is high probability of the existence of the $Pa{-}3 \rightarrow Pm{-}3m$ phase transformation. Recently, such a transformation was detected for the related tungsten double oxofluoride salt $(NH_4)_3WO_2F_5$ [13].

Search of the possible PT and the study of the $(NH_4)_3SnF_7 = (NH_4)_3[SnF_6]F = (NH_4)_2SnF_6{\cdot}NH_4F$ crystal structure in a wide temperature range were the main objectives of the present work. Hereinafter, we will use the $(NH_4)_3SnF_7$ formula for this compound.

* Corresponding author at: L.V. Kirensky Institute of Physics, Siberian Branch of RAS, 660036 Krasnoyarsk, Russia.
E-mail address: msmolokeev@gmail.com (M.S. Molokeev).

http://dx.doi.org/10.1016/j.jfluchem.2015.06.024
0022-1139/© 2015 Elsevier B.V. All rights reserved.

2. Synthesis and crystal growth

Colorless single crystals of ammonium heptafluorostannate $(NH_4)_3SnF_7$ were obtained from fluoride aqueous solution of $(NH_4)_2SnF_6$ and NH_4F. The method is quite different from that described earlier [4], which comprised the interaction of elemental tin with NH_4HF_2 at 300 °C. We used the metallic tin platelets (β-Sn) of the 99.9% purity as a starting material for synthesis of $(NH_4)_2SnF_6$. Such a synthesis has been previously described in [14], where the starting reagent was freshly precipitated meta-tin acid. We used chemically pure nitric acid (56 mass. % HNO_3) and hydrofluoric acid (40% HF) for tin oxidation and complexation in accordance with the reaction:

$$Sn + 6HF + 4HNO_3 = H_2SnF_6 + 4NO_2 + 4H_2O.$$

Tin platelets were chemically etched in the excess of HF with accurate dropwise addition of HNO_3 at room temperature because of high exothermal character of the above reaction. The solution pH was about 0, then NH_3·aq (25%) was added to attain pH 2:

$$H_2SnF_6 + 2NH_3 = (NH_4)_2SnF_6.$$

During evaporation, thin hexagonal plates of $(NH_4)_2SnF_6$ were formed (the PXRD pattern were matching with the JCPDS file No. 026-0094): they were further used for the synthesis of $(NH_4)_3SnF_7$. The large excess of NH_4F is needed relative to stoichiometry:

$$(NH_4)_2SnF_6 + NH_4F = (NH_4)_3SnF_7.$$

At least, a triple excess of NH_4F was taken to obtain polyhedral single crystals of the double salt during evaporation of the solution. The obtained crystals were rinsed with ethanol under vacuum and air-dried.

3. Differential scanning calorimetric measurements

Since the room temperature phase of $(NH_4)_3SnF_7$ was characterized as a cubic one (sp. gr. $Pm-3m$) [4], the probable PT associated with the symmetry lowering would be expected to exist at a decreased temperature. On the other hand, the higher temperature studies of heptafluorostannate were also performed with respect to a possible decomposition of $(NH_4)_3SnF_7$ to $(NH_4)_2SnF_6$, similarly to $(NH_4)_3TiF_7$ at 380 K [10].

In order to examine the possible anomalous behavior of $(NH_4)_3SnF_7$, heat capacity measurements were carried out using a DSM-10 M differential scanning microcalorimeter (DSM) in a wide temperature range 100–420 K as the first stage of study. The compound under study was put into an aluminum sample holder. Temperature and enthalpy were calibrated using the melting parameters of pure indium. The temperatures were determined with an accuracy of ±1 K and the uncertainty on the enthalpy value was estimated as ±5 J mol^{-1}. The experiments were carried out in a He gaseous atmosphere. The heating and cooling rates were fixed at 8 K min^{-1}. Heat capacity $C_p(T)$ measurements were performed on several powdered samples from the same crystallization experiment. The mass of the samples was about 0.06–0.10 g.

No heat capacity anomalies were found below room temperature. Consequently, the cubic phase of $(NH_4)_3SnF_7$ was stable down to at least 100 K, which was the lowest temperature in calorimetric experiments.

As regards measurements above room temperature, a reversible anomalous behavior of $C_p(T)$ was observed. Fig. 1 depicts the temperature dependence of the excess heat capacity ΔC_p obtained as a difference between the total heat capacity C_p and non-anomalous lattice contribution C_{lat}. On heating as well as on cooling, it was possible to see one anomaly with a maximum at about 360 K. One could assume that such anomalous behavior was associated with the decomposition of double salt $(NH_4)_3SnF_7$ to $(NH_4)_2SnF_6$ with the isolation of NH_4F (NH_3 + HF), which was observed for the related heptafluorotitanate [11]. However, the reversibility of the $\Delta C_p(T)$ anomalous dependence at repeated heating and cooling indicates unambiguously that this phenomenon is not related exclusively to the decomposition of $(NH_4)_3SnF_7$. Moreover, only a small decrease of the samples mass (by about 0.4%) was found after heating-cooling cycles. Thus, it was supposed that the heat phenomenon observed was associated with structural phase transition. The enthalpy change at this transformation was found as $\Delta H = \int \Delta C_p dT = 6000 \pm 800$ J mol^{-1}. The rather large error value was due to the enthalpy change from sample to sample.

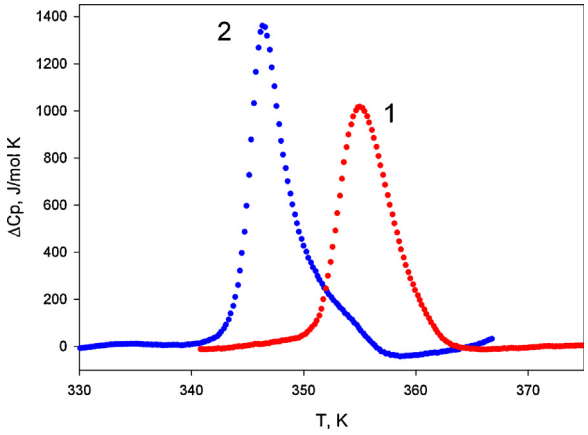

Fig. 1. Temperature dependence of the anomalous heat capacity of (NH4)3SnF7 measured upon heating (1) and cooling (2).

4. Optical observations

In the second stage, the examination of a cubic phase stability was performed by optical studies with an "Axioskop-40" polarizing microscope and a "Linkam LTS 350" temperature chamber in a wide temperature range of 90–450 K. Upon cooling, starting from room temperature, $(NH_4)_3SnF_7$ remains optically isotropic down to 90 K.

In order to avoid the possible decomposition of $(NH_4)_3SnF_7$, as was observed in the case of $(NH_4)_3TiF_7$ [11], high temperature optical investigations were carried out on the crystal plate placed in oil under cover glass. Fig. 2 shows the transformation of the picture observed using a microscope in the process of heating.

At room temperature, the crystal is optically isotopic in accordance with its cubic symmetry (Fig. 2a). Upon heating, at $T_{0\uparrow} = 360 \pm 1$ K the cracks appear on the surface of the crystal plate (Fig. 2b): they are collapsed along with small temperature increase. Above T_0, the crystal remains optically isotropic. Upon cooling, the cracking occurs at $T_{0\downarrow} = 359 \pm 1$ K and the crystal recovers its monolithic state.

Heating in the range from 370 up to 380 K leads again to the appearance of microcracks on the crystal plate surface, of which gas bubbles go out in oil (Fig. 2c). Thereafter, the microcracks vanish. Annealing of the crystal plate for three hours at $T = 373$ K results in the completion of gassing process. It was supposed that gas was water vapor absorbed in crystal defects during the crystal growth process. As a corroboration of this assumption, one can see a photograph of ice microcrystals formed in the defect holes of the crystal below 240 K (Fig. 3). The sample is not recovered after heating above 420 K.

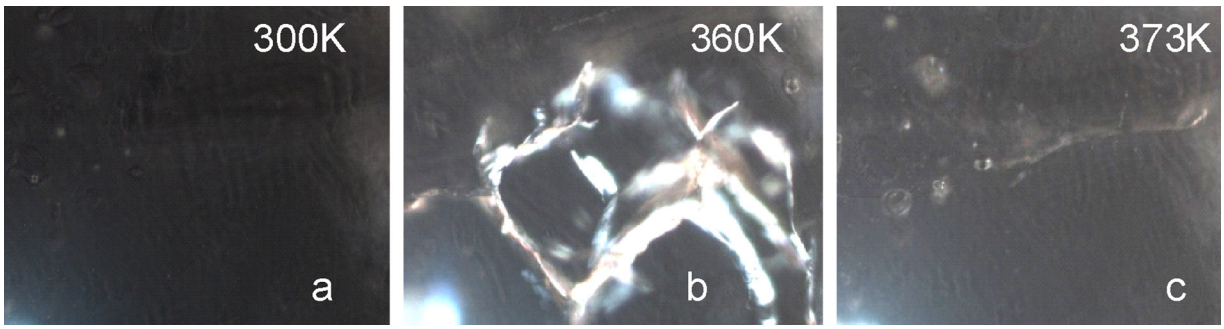

Fig. 2. Observation of the $(NH_4)_3SnF_7$ crystal in polarized light under heating and cooling process. The small bubbles with vapor can be seen in (b, c).

Unchanged optical isotropy of $(NH_4)_3SnF_7$ means that cubic symmetry remains stable over the whole temperature range studied. Taking into account the reversible anomalous behavior of the heat capacity near 360 K, it is evident that this double salt undergoes PT between cubic phases as was suggested, for example, for $(NH_4)_3ZrF_7$ with seven-coordinated zirconium polyhedron [15].

5. X-ray investigations

5.1. Powder X-ray data of G_1 and G_0 phases

The powder diffraction data of $(NH_4)_3SnF_7$ for Rietveld analysis were collected using a Bruker D8 ADVANCE powder diffractometer (Cu-Kα radiation) and linear VANTEC detector. The beam was controlled by the 0.6 mm fixed divergence slit, 6 mm receiving VANTEC slit, and Soller slits. The step size of 2θ was 0.016°. An Anton Paar TTK450 accessory was used for low- and high-temperature measurements.

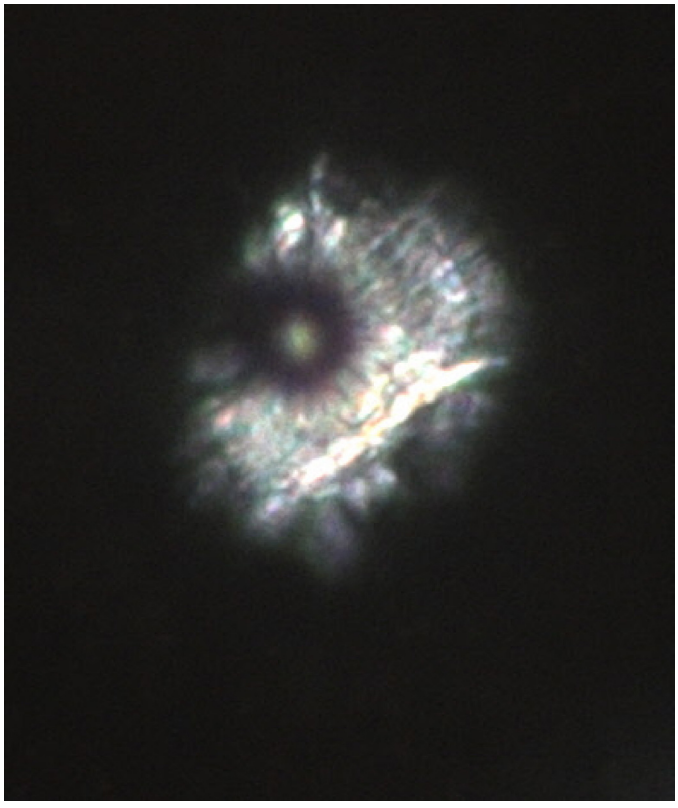

Fig. 3. Formation of optically anisotropic ice crystals in spherical holes of unannealed sample of $(NH_4)_3SnF_7$ at temperatures below 240 K.

Fifteen patterns were collected from 143 K to 403 K (Fig. 4). One can see that powder patterns at T = 373 K and higher temperatures show disappearing of small superstructure peaks of the main phase of $(NH_4)_3SnF_7$ and simultaneous emergence of peaks corresponding to the impurity phase of $(NH_4)_2SnF_6$ (Fig. 4). Initially, it was difficult to understand whether disappearing of superstructure peaks corresponded to the compound decomposition or to the structural phase transition. In order to shed light upon this problem, the additional series of experiments were performed between 303 and 369 K in heating and cooling modes (Fig. 5). The results clearly show reversible disappearing and appearing of superstructure peaks upon heating and cooling, respectively. In the case of decomposition process solely, the superstructure peaks could not appear again. Thus, the change of the X-ray powder diffraction patterns along with temperature corroborates the existence of structural PT in $(NH_4)_3SnF_7$ accompanied by the decomposition process followed by the emergence of the $(NH_4)_2SnF_6$ phase.

Analysis of the structural peak (0 2 2) shows that it splits into two peaks below PT upon heating and above PT upon cooling (Fig. 6). However, one can see that such a splitting is absent in high temperature phase G_0. All other structural peaks have similar behavior upon heating and cooling. The presence of reflection splitting only near the PT point means that high G_0 and low G_1 temperature phases belong to the same crystal system and both of them coexist in the narrow temperature range close to that of structural transformation.

The data obtained for the phase G_0 are in contradiction with the results obtained earlier [4] where the cubic structure $Pm\bar{3}m$ (a = 5.980(1) Å) was postulated at room temperature for $(NH_4)_3SnF_7$. Simulation of the X-ray pattern obtained at

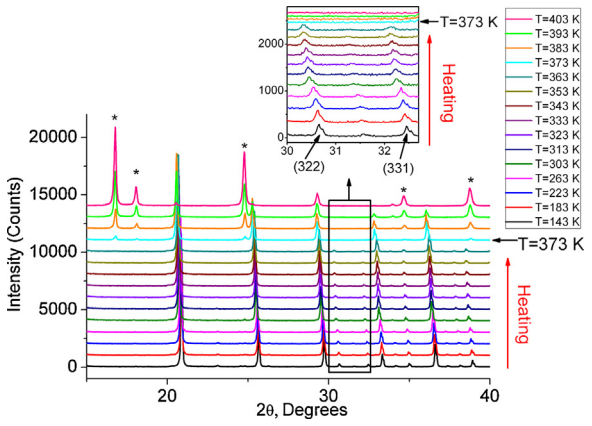

Fig. 4. X-ray powder patterns of $(NH_4)_3SnF_7$ at different temperatures from 143 K to 403 K. Inset shows disappearing of superstructure peaks (3 2 2) and (3 3 1) at T = 373 K under heating. Peaks of impurity phase of $(NH_4)_2SnF_6$ appeared at T = 373 K are marked with an asterisk.

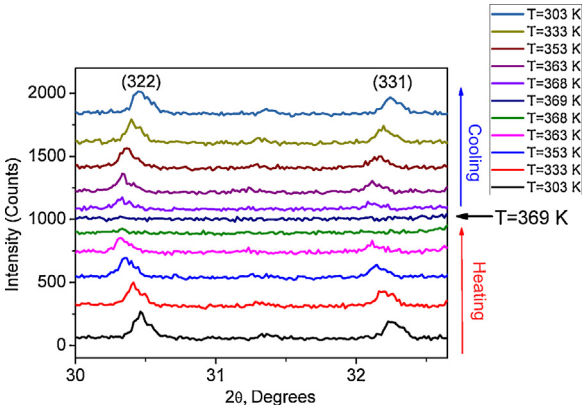

Fig. 5. Fragment of X-ray powder patterns of $(NH_4)_3SnF_7$ with superstructure peaks (3 2 2) and (3 3 1) on heating and cooling.

T = 303 K shows that several small peaks can not be accounted by this cell. We believe that these peaks are related to the superstructure and do not correspond to impurity phase, since they disappear and appear at PT upon heating and cooling, respectively (Figs. 4 and 5). To account these peaks, the doubling of the unit cell parameter ($a = 2 \times 5.980$ Å) was implemented. Analysis of extinction rules uniquely gives the space group $Pa{-}3$ for the G_1 low temperature phase similarly to that of $(NH_4)_3TiF_7$ below T_2 [9]. After that all peaks were indexed by this transformed cell. At PT the intensity of superstructure peaks diminished and the G_0 structure was fitted very reliably by cubic symmetry $Pm{-}3m$ (a = 5.980(1) Å) [4].

Since the room temperature phase G_1 of $(NH_4)_3SnF_7$ has similar cell parameters and space group with $(NH_4)_3TiF_7$ below T_2, it was suggested to use the crystal structure of the latter as a starting model to refine the structure of $(NH_4)_3SnF_7$. The Rietveld refinement using TOPAS 4.2 [16] was stable and gave low R-factors (Table 1, Fig. 7). The atomic coordinates are summarized in Table 1S.

All peaks of high temperature pattern at T = 373 K can be assigned to two phases: (1) main G_0 phase ($Pm{-}3m$) of $(NH_4)_3SnF_7$; and (2) small amount of impurity phase of $(NH_4)_2SnF_6$. Therefore, we performed the refinement of both phases. The crystal structure [4] was used as a starting model for refinement of the G_0 phase. The F3 atom (Fig. 8a) in the previous model [4] was placed in the 8 g Wyckoff site. However, in such a case it is impossible to build octahedra using all eight F atoms, which can be generated from F3. In this case, an ideal cubic polyhedron SnF_8 can be built instead of octahedron SnF_6. Therefore, it was suggested to move the F3 atom from the 8 *g* site to the 24*m* one in order to get four disordered SnF_6 octahedra instead of one cube. Refinement was stable and gave low

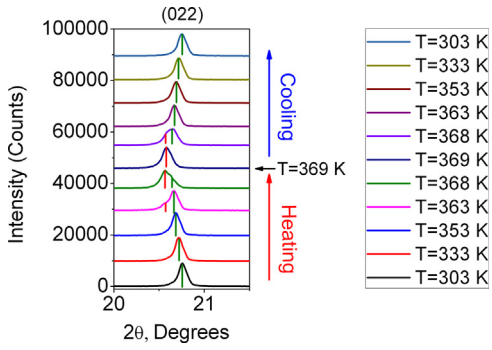

Fig. 6. Fragment of X-ray powder patterns of $(NH_4)_3SnF_7$ with structure peak (0 2 2) on heating and cooling. Green sticks correspond to the low temperature phase G_1, red sticks to the high temperature phase G_0.

Table 1
Main parameters of Rietveld refinement of the $(NH_4)_3SnF_7$ sample in two phases.

Phase	G_1	G_0
Temperature, K	303	373
Sp. Gr.	$Pa{-}3$	$Pm{-}3m$
a, Å	12.08950(7)	6.09238(7)
V, Å^3	1766.95(3)	226.132(8)
Z	8	1
2θ-interval,°	5–120	5–120
Number of reflections	447	54 (main phase) + +105 (impurity)
Number of parameters of refinement	44	49
R_{wp}, %	8.22	12.15
R_p, %	6.38	9.13
R_{exp}, %	5.08	9.30
χ^2	1.62	1.31
R_B, %	3.24	3.74

R-factors (Table 1, Fig. 9). The atomic coordinates are presented in Table 1S. Further details of the crystal structure can be obtained from Fachinformationszentrum Karlsruhe, 76344 Eggenstein-Leopoldshafen, Germany (fax: (+49)7247 808 666; E-mail: crystdata@fiz-karlsruhe.de; http://www.fiz-karlsruhe.de/request_for_deposited_data.html on quoting the deposition number CSD-429520 and the supporting information containing the CIF file.

Hydrogen atoms were not located in the G_0 phase because the NH_4 group must be disordered at least between two positions due to high 4/*mmm* symmetry of its crystallographic site (3*c*). X-ray powder diffraction is not a good tool to locate H atoms in such a case. It seems that even disordering of SnF_6 octahedron cannot be defined absolutely reliably from these experiments. On the other

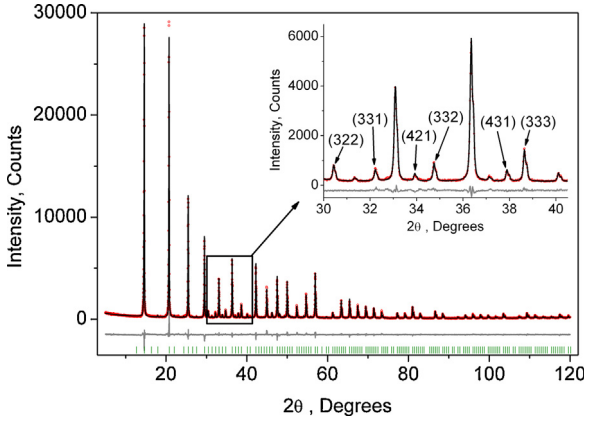

Fig. 7. Difference Rietveld plot of $(NH_4)_3SnF_7$ at T = 303 K in G_1 phase ($Pa{-}3$). Insert shows some superstructure peaks which are prohibited in G_0 phase ($Pm{-}3m$).

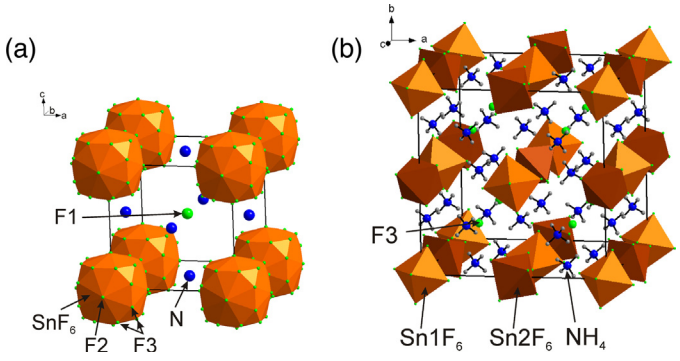

Fig. 8. Crystal structure of $(NH_4)_3SnF_7$: (a) G_0 phase at T = 373 K; (b) G_1 at T = 303 K.

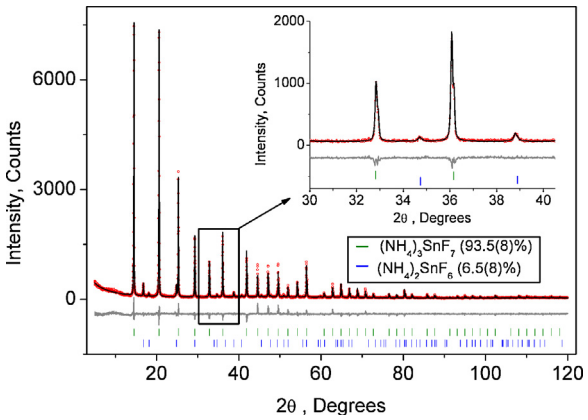

Fig. 9. Difference Rietveld plot of $(NH_4)_3SnF_7$ at $T = 373$ K in G_0 phase ($Pm-3m$). Inset shows the absence of superstructure peaks and the appearance of small amount of impurity phase $(NH_4)_2SnF_6$.

hand, the fact of disordering can be stated surely for several reasons: (1) very high symmetry $m-3m$ of the Sn site (1*a*); (2) several maximums of electron density at appropriate Sn–F distance in addition to the ideal position of the octahedron were located in our experiments and in the single crystal experiment [4]; (3) the structure of G_1 phase ($Pa-3$) (Fig. 8b) shows that SnF_6 should be highly disordered to form G_0 phase ($Pm-3m$) (Fig. 8a).

All patterns from 143 to 403 K were treated in a similar way and the temperature dependence of cell parameters (Fig. 10a) and cell volume (Fig. 10b) were plotted. A rather large jump in the volume of formula unit at PT ($\Delta V = 3.05$ Å^3; $\Delta V/V \approx 1.3\%$) points that the

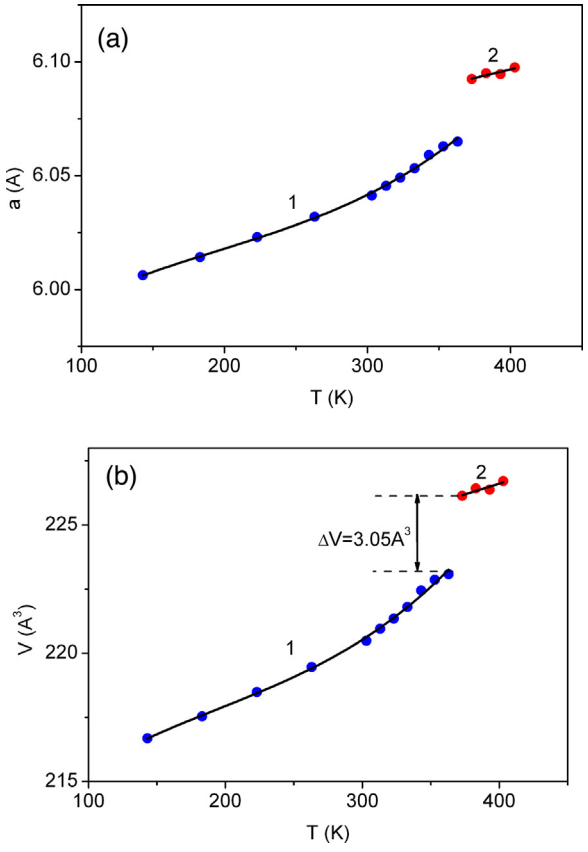

Fig. 10. Temperature dependence of the: a) cell parameters: (1) $a/2$ in G_1 phase; (2) a in G_0 phase; (b) formula unit volume (V/Z): (1) G_1 phase ($Z = 8$); (2) G_0 phase ($Z = 1$).

$G_0 \leftrightarrow G_1$ PT in $(NH_4)_3SnF_7$ is a transformation of the strong first order.

5.2. Single crystal data of G_1 phase

The single crystal data were measured to prove $Pa-3$ space group of the G_1 phase only at room temperature due to crystal crashes upon heating above PT point. The intensities were collected at 293 K using a SMART APEX II X-ray single crystal diffractometer (Bruker AXS) equipped with a CCD-detector, graphite monochromator, and MoKα radiation source. The exposure time was 20 s per each frame; the distance from crystal to detector was 45 mm. All data processing and refinement of cell parameters were performed using program Apex II [17]. The crystal structure was solved and refined using programs SHELXTL/PC [18].

Careful check of reflections in diffraction space shows the existence of additional superstructure reflections with $I > 3\sigma$, which cannot be indexed by the $Pm-3m$ phase. Therefore, the single crystal data also prove a doubling of cell parameters at room temperature. Analysis of extinction rules and statistics of reflection intensities confirmed the $Pa-3$ space group of the G_1 phase. So, one can see a good agreement between powder and single crystal data.

All non-hydrogen atoms of the G_1 phase were found by direct method and refined with anisotropic thermal parameters. All hydrogen atoms were localized on the electron difference map and were not refined. Data measurement and processing are presented in Table 2, atomic coordinates are given in Table 2S, some bond lengths and angles are in Table 3S. The parameters of hydrogen bonds are presented in Table 4S. Further details of the crystal structure can be obtained from Fachinformationszentrum Karlsruhe on quoting the deposition numbers: CSD-429519.

6. Discussion

The main results of $(NH_4)_3SnF_7$ investigations are as follows: (1) the room temperature phase was refined on powder and single crystal samples as a cubic one with the symmetry $Pa-3$ contrary to $Pm-3m$ suggested in [4]; (2) a reversible PT between two cubic phases $Pa-3 \leftrightarrow Pm-3m$ was found at 360 K. The first point means that the increase of the ionic radius of a central atom from Ti (0.605 Å) to Sn (0.690 Å) leads to strong enlargement of the temperature range of the $Pa-3$ phase stability in $(NH_4)_3SnF_7$

Table 2
Single crystal experimental data for $(NH_4)_3SnF_7$ in G_1 phase at room temperature.

Crystal data	
Phase	G_1
Sp. Gr.	$Pa-3$
a, Å	12.0866(1)
V, Å^3	1765.68(3)
Z	8
D_x, Mg × m^{-3}	2.301
μ, mm^{-1}	2.962
Crystal size, mm	0.20 × 0.19 × 0.18
Data collection	
Temperature, K	296
Radiation type	Mo Kα
T_{min}, T_{max}	0.6177, 0.5888
No. of measured, independent and observed [$I > 2\sigma(I)$] reflections	81577, 2045, 1003
R_{int}	0.0249
θ_{max} (°)	41.85
Refinement	
$R[F^2 > 2\sigma(F^2)]$, $wR(F^2)$, S	0.0254, 0.0720, 1.057
No. of parameters	36
$\Delta\rho_{max}$, $\Delta\rho_{min}$ (e Å^{-3})	1.150, −0.928

compared to $(NH_4)_3TiF_7$ [12]. The second point is in good agreement with the results of the *T–p* phase diagram study of heptafluorotitanante where such a structural transformation was suggested at a pressure above 0.41 GPa [12].

The microscopic studies of $(NH_4)_3SnF_7$ shows an active cracking of the sample at PT point $T_{0\uparrow} = 360 \pm 1$ K; $T_{0\downarrow} = 359 \pm 1$ K with further repairs of its monolith upon both heating and cooling processes. The cracks appear due to very large jump of the unit cell volume (Fig. 10). It is an intriguing case of structural transformation of the first order which is accompanied by the low temperature hysteresis and large volume change.

Low temperature *Pa*−3 phase of $(NH_4)_3SnF_7$ is ordered because all SnF_6 octahedra are ordered and NH_4 tetrahedra seem to be ordered as well. However, the *Pm*−3*m* phase has the highest degree of disordering. Indeed, the NH_4 group is disordered in *Pm*−3*m* at least between two positions according to the *4/mmm* symmetry. However, the possibility of higher disorder degree of tetrahedral cations should not be excluded. Two nonequivalent SnF_6 octaherda with different orientations ($Sn1F_6$ and $Sn2F_6$) in *Pa*−3 phase (Fig. 8b) occupy one site in *Pm*−3*m* phase and one of them becomes disordered. Counting the number of different oriented octahedra in *Pa*−3 formula unit shows that there are four $Sn1F_6$ and four $Sn2F_6$ octahedra (Fig. 8b). In the *Pm*−3*m* phase, each $Sn2F_6$ octahedron is disordered between four positions, leading to 3.8^2 polyhedron, however, the Sn1F6 octahedron is ordered due to its specific orientation. Therefore, the SnF_n polyhedron in the *Pm*−3*m* phase (Fig. 8a) can be decomposed into SnF_6 octahedron and 3.8^2 polyhedron [4] having equal probabilities of their existence $P = 1/2$ (Fig. 11). Similar 3.8^2 polyhedron was also observed in $(NH_4)_3TiF_7$ [11]. Therefore, it can be decomposed into four SnF_6 octahedra with different orientations (Fig. 11). As far as the existence probability of 3.8^2 polyhedron is equal to 1/2, the one of each of the four SnF_6 octahedra is equal to $(1/2) \times (1/4) = 1/8$. Therefore, SnF_6 octahedra in the G_0 phase are disordered between 4 + 1 = 5 positions with different probabilities $P = 1/8$ and $P = 1/2$ (Fig. 11).

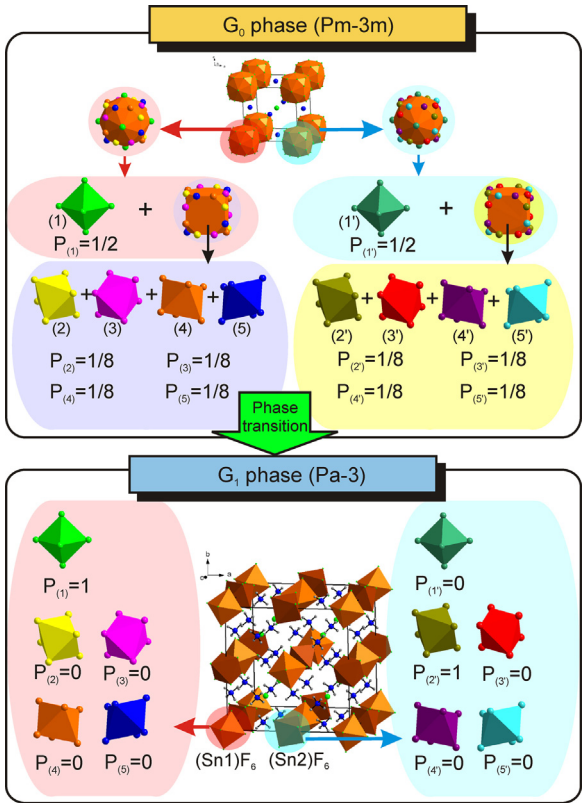

Fig. 11. Model of ordering of the (Sn1)F6 and (Sn2)F6 octahedra. Numbers Pi under particular orientation of the octahedron indicate to the probability of its existence.

The crystal structure of distorted *Pa*−3 phase was decomposed into symmetry modes of the parent structure *Pm*−3*m* using program ISODISTORT [19], and five modes were revealed: $\Gamma_1^+(\eta)$; $M_5^+(\varepsilon, 0, \varepsilon, 0, \varepsilon, 0)$; $X_5^+(\xi, 0, \xi, 0, \xi, 0)$; $R_1^+(\chi)$ and $R_2^+(\sigma)$ with **k** vectors [0,0,0], [1/2, 1/2, 0], [0, 1/2, 0] [1/2, 1/2, 1/2] and [1/2, 1/2, 1/2], respectively. The η, ε, ξ, χ and σ are order parameters, which are transformed according to the irreducible representations of the space group *Pm*−3*m*. ISODISTORT shows that only $X_5^+(\xi, 0, \xi, 0, \xi, 0)$ are the critical modes which drive phase transition, that can be written as:

$$Pm{-}3m \rightarrow \{X_5^+(\xi, 0, \xi, 0, \xi, 0)\} \rightarrow Pa{-}3$$

By integration of the $(\Delta C_p/T)(T)$ function, the value of the total entropy change associated with the phase transition in $(NH_4)_3SnF_7$ was determined as $\Delta S = 16.6 \pm 2.5$ J mol^{-1} K. Such a large value of entropy change ($\Delta S \approx 2$ R, where R is gas constant) is characteristic for phase transitions of the order-disorder type. These results are in a good agreement with the structural refinement data above where the disorder of hexaflurostannate octahedra as well of ammonium tetrahedra was proved for *Pm*−3*m* phase. It is necessary to point out that the DSM-method is not always able to give exact information about the pre-transitional heat effects, particularly when a rather small excess heat capacity exists in a wide temperature range below the phase transition point as it was found, for example, in case of the related $(NH_4)_3TiF_7$ [12]. That is why we do not discuss the entropy parameter in the framework of the structural ordering model suggested above. To get more exact data about entropy changes, the investigations by an adiabatic calorimeter are in progress.

7. Conclusion

Calorimetric, optic, and X-ray studies have revealed that the double salt $(NH_4)_3SnF_7$ undergoes the first order PT between two cubic phases *Pa*−3 ↔ *Pm*−3*m* at about 360 K. These results are consistent with the *T–p* phase diagram for the related heptafluorotitanate where a possibility of such a transformation was suggested at pressure above 0.41 GPa [12] and are also supported by similar transformation in the case of $(NH_4)_3WO_2F_5$ [13]. Hence, contrary to [4], it was found that the increase of the central atom size from Ti to Sn resulted in strong broadening of the temperature range of the *Pa*−3 cubic phase stability. The distortion of structure is accompanied by a rather large unit cell volume jump (~1.3%) leading to the destruction of the single crystal sample. The results of structural analysis have shown that octahedral SnF_6 and tetrahedral NH_4 groups are ordered in *Pa*−3 phase, while they are disordered in the *Pm*−3*m* phase. The large entropy change at phase transition point agrees well with an order-disorder transformation.

Acknowledgements

We thank T.A. Kaidalova for the idea of doubling the unit cell parameter of $(NH_4)_3SnF_7$ at room temperature. The reported study was partially supported by RFBR, research project No. 15-02-02009 a.

Appendix A. Supplementary data

Supplementary data associated with this article can be found, in the online version, at http://dx.doi.org/10.1016/j.jfluchem.2015.06.024.

References

[1] B. Hofmann, R. Hoppe, Z. Anorg. Allg. Chem. 458 (1979) 151–162.
[2] D.L. Deadmore, W.F. Bradley, Acta Cryst. 15 (1962) 186–189.
[3] C. Plitzko, G. Meyer, Z. Krist, New Cryst. Struct. 213 (1998) 475.
[4] C. Plitzko, G. Meyer, Z. Anorg. Allg. Chem. 623 (1997) 1347–1348.
[5] J.L. Hoard, M.B. Williams, J. Am. Chem. Soc. 64 (1942) 633–637.
[6] U. Reusch, E. Schweda, Mater. Sci. Forum 378 (2001) 326–330.
[7] R.L. Davidovich, L.P. Voskresenskaya, T.A. Kaidalova, Bull. Acad. Sci. USSR Chem. Sci. 21 (2) (1972) 230–233.
[8] R. Hoppe, Angew. Chem. Int. Ed. Engl. 20 (1981) 63–87.
[9] W. Massa, D. Babel, Chem. Rev. 88 (1988) 275–296.
[10] S.V. Mel'nikova, E.I. Pogoreltsev, I.N. Flerov, N.M. Laptash, J. Fluorine Chem. 162 (2014) 14–19.
[11] M.S. Molokeev, S.V. Misjul, I.N. Flerov, N.M. Laptash, Acta Cryst. B70 (2014) 924–931.
[12] E.I. Pogoreltsev, I.N. Flerov, A.V. Kartashev, E.V. Bogdanov, N.M. Laptash, J. Fluorine Chem. 168 (2014) 247–250.
[13] A.A. Udovenko, N.M. Laptash, Acta Crystallogr. B71 (2015), http://dx.doi.org/10.1107/S2052520615010835 (in press).
[14] R.L. Davidovich, T.A. Kaidalova, Russ. J. Inorg. Chem. 16 (1971) 2539–2541.
[15] V.D. Fokina, M.V. Gorev, E.V. Bogdanov, E.I. Pogoreltsev, I.N. Flerov, N.M. Laptash, J. Fluorine Chem. 154 (2013) 1–6.
[16] Bruker AXS TOPAS V4: General Profile and Structure Analysis Software for Powder Diffraction Data. User's Manual, Bruker AXS, Karlsruhe, Germany, 2008.
[17] APEX 2, Version 2008, Bruker AXS Inc., Madison, WI, 2008.
[18] G.M. Sheldrick, Acta. Crystallogr. A64 (2008) 112–122.
[19] B.J. Campbell, H.T. Stokes, D.E. Tanner, D.M. Hatch, J. Appl. Cryst. 39 (2006) 607–614.